ResearchGate

See discussions, stats, and author profiles for this publication at: https://www.researchgate.net/publication/49652987

Magnetic Field Effect Corroborated with Docking Study to Explore Photoinduced Electron Transfer in Drug–Protein Interaction

ARTICLE *in* THE JOURNAL OF PHYSICAL CHEMISTRY A · DECEMBER 2010

Impact Factor: 2.69 · DOI: 10.1021/jp109604a · Source: PubMed

CITATIONS
22

READS
42

4 AUTHORS, INCLUDING:

Brotati Chakraborty
Bejoy Narayan Mahavidyalaya, Itachuna, H…
12 PUBLICATIONS **126** CITATIONS
SEE PROFILE

Atanu Singha Roy
National Institute of Technology, Meghalaya
19 PUBLICATIONS **181** CITATIONS
SEE PROFILE

Swagata Dasgupta
IIT Kharagpur
121 PUBLICATIONS **1,736** CITATIONS
SEE PROFILE

Available from: Brotati Chakraborty
Retrieved on: 27 January 2016

Magnetic Field Effect Corroborated with Docking Study to Explore Photoinduced Electron Transfer in Drug−Protein Interaction

Brotati Chakraborty,[†] Atanu Singha Roy,[‡] Swagata Dasgupta,[‡] and Samita Basu*[,†]

Chemical Sciences Division, Saha Institute of Nuclear Physics, 1/AF Bidhannagar, Kolkata-700064, India, and Department of Chemistry, Indian Institute of Technology, Kharagpur-721302, India

Received: June 14, 2010; Revised Manuscript Received: November 4, 2010

Conventional spectroscopic tools such as absorption, fluorescence, and circular dichroism spectroscopy used in the study of photoinduced drug−protein interactions can yield useful information about ground-state and excited-state phenomena. However, photoinduced electron transfer (PET) may be a possible phenomenon in the drug−protein interaction, which may go unnoticed if only conventional spectroscopic observations are taken into account. Laser flash photolysis coupled with an external magnetic field can be utilized to confirm the occurrence of PET and authenticate the spin states of the radicals/radical ions formed. In the study of interaction of the model protein human serum albumin (HSA) with acridine derivatives, acridine yellow (AY) and proflavin (PF^+), conventional spectroscopic tools along with docking study have been used to decipher the binding mechanism, and laser flash photolysis technique with an associated magnetic field (MF) has been used to explore PET. The results of fluorescence study indicate that fluorescence resonance energy transfer takes place from the protein to the acridine-based drugs. Docking study unveils the crucial role of Ser 232 residue of HSA in explaining the differential behavior of the two drugs towards the model protein. Laser flash photolysis experiments help to identify the radicals/radical ions formed in the due course of PET ($PF^•$, $AY^{•-}$, $TrpH^{•+}$, $Trp^•$), and the application of an external MF has been used to characterize their initial spin-state. Owing to its distance dependence, MF effect gives an idea about the proximity of the radicals/radical ions during interaction in the system and also helps to elucidate the reaction mechanisms. A prominent MF effect is observed in homogeneous buffer medium owing to the pseudoconfinement of the radicals/radical ions provided by the complex structure of the protein.

1. Introduction

Literature survey shows that nowadays photoinduced drug−protein interaction is being extensively studied by ultraviolet−visible (UV−vis) absorption spectroscopy, steady-state fluorescence spectroscopy, and circular dichroism (CD) spectroscopy to look into ground-state complex formation, excited state phenomenon such as fluorescence resonance energy transfer (FRET), and perturbation of the secondary structure of a protein by a drug, respectively.[1−4] However, drug−protein interaction may also involve photoinduced electron transfer (PET), which may go unnoticed if only the conventional spectroscopic investigations are taken into account. Although PET reactions in proteins[5−10] have already been reported by a number of workers, especially intramolecular PET, relatively little is known about PET in drug−protein interaction. In order to confirm the occurrence of PET, identification and characterization of radical or radical ions, which are formed as primary intermediates, is necessary. Laser flash photolysis is an efficient tool to identify such radicals/radical ions that are formed in the due course of PET. However, mere identification of radicals/radical ions does not give the complete information regarding PET, such as the original spin-state of the radicals/radical ions and also the proximity of the radicals/radical ions during interaction in the system.

A weak magnetic field (MF) on the order of 0.01−0.08 T has an immense potential to elucidate PET reactions by characterization of radicals or radical ions formed in the due course of reaction, which are affected by the presence of MF as they contain free electrons. The electron spin multiplicity of the excited state is generally preserved during the charge transfer, and the memory of this initial spin multiplicity is retained in the resulting radical pairs (RPs)/radical ion pairs (RIPs) until the latter undergoes further reactions. As the RIP is a "spin selective microreactor", the nature of the product formed is spin-dependent.[11] The spin multiplicity of the RIP, however, is not stationary and can evolve coherently between the singlet (S) and triplet (T) configurations. An applied MF can alter the fate of a PET reaction by influencing this spin evolution in spite of contributing nothing to the chemical energy. Observation of MF effect (MFE) is a composite effect of diffusion dynamics, spin dynamics and recombination or free radical formation.[12−19] The three T states ($T_±$, T_0) are degenerate in the absence of an external field. The energies of the S and T states, however, differ by $2J$, where J is the electron exchange integral that preserves electron indistinguishability. J depends on the separation between the two RP centers and falls off exponentially as the components of the RIP diffuse apart. The RIPs of the geminate-cage diffuse to an optimum distance of separation where $2J$ is almost zero, and eventually there is an effective mixing of the S and the ($T_±$, T_0) states (as depicted in Figure 1a) via hyperfine coupling mechanism. Under this condition, if an external MF on the order of hyperfine interaction (HFI) or higher is applied, the degeneracy of the triplet states is removed (popularly known

* Corresponding author. Telephone: +91-33-2337-5345. Fax: +91-33-2337-4637. E-mail: samita.basu@saha.ac.in. Address: Chemical Sciences Division, Saha Institute of Nuclear Physics, 1/AF Bidhannagar, Kolkata-700064, India.
[†] Saha Institute of Nuclear Physics.
[‡] Indian Institute of Technology.

10.1021/jp109604a © 2010 American Chemical Society
Published on Web 12/02/2010

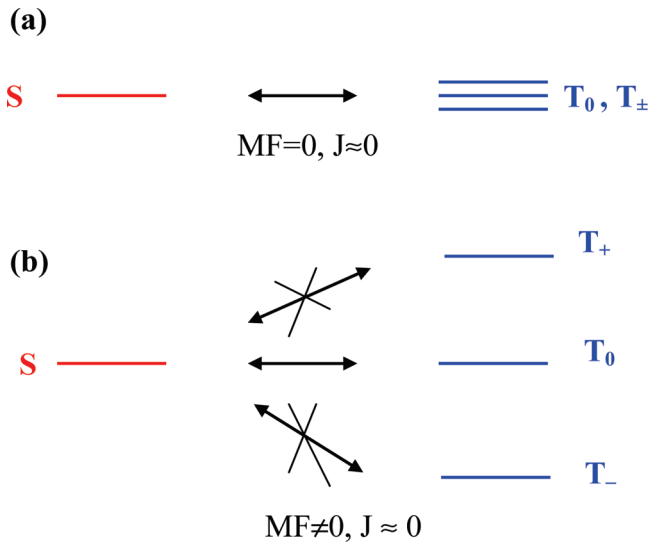

Figure 1. (a) Energy levels of degenerate singlet (S) and three triplet states (T_0, $T_\pm$) in the absence of an external MF. (b) Energy levels of S and T states in the presence of an external MF; removal of degeneracy of the T states due to Zeeman splitting allows only S → T_0 transition.

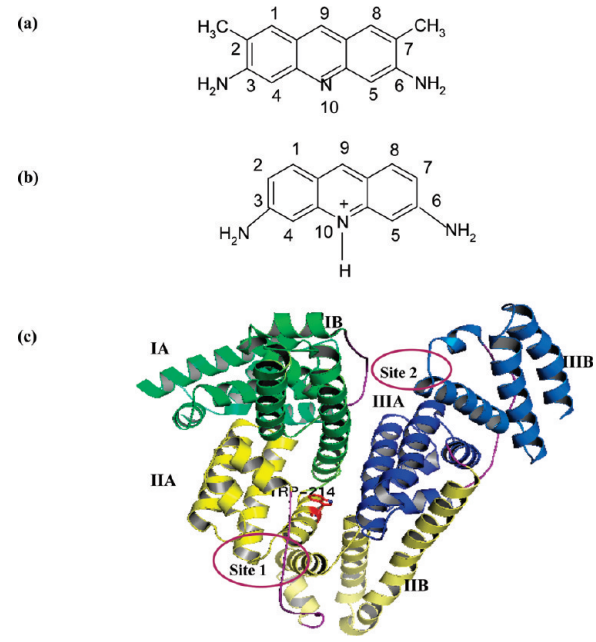

Figure 2. (a) Chemical structure of AY. (b) Chemical structure of PF^+. (c) Crystal structure of HSA.

as Zeeman effect) and thus the probability of intersystem crossing (ISC) is reduced since only the S → T_0 channel is operative (as shown in Figure 1b), which results in the increase in population of the initial spin state. In fact, the external MF competes with the internal MF (i.e., HFI present in the system) to control the spin-rephasing rate of solvent separated ion pairs. The modulation in spin dynamics can be detected either by monitoring the exciplex luminescence of singlet precursors or by using laser flash photolysis technique on the triplet nonfluorescent precursors. Usually, geminate RPs/RIPs with singlet correlation lead to the formation of recombination product or exciplex, whereas those with triplet configuration prefer to form escape product (free radicals/radical ions). As a consequence, if the initial spin state of the RPs/RIPs is singlet, then there will be an enhancement in the luminescence of the singlet precursors, whereas, if the initial spin state is triplet, then the absorbance of the triplet precursors will increase. Thus, MFE helps to identify the parent spin state of the radical or radical ions. Moreover, MFE is very sensitive to the distance between the participating radicals/radical ions because the hyperfine induced spin flipping depends on *J*, which in turn is exponentially distance dependent. When the radicals/radical ions are in contact, the S−T splitting caused by *J* is much stronger than the hyperfine coupling energies so that spin evolution cannot occur by this mechanism. On the other hand, at a distance where 2*J* is sufficiently small, S−T conversion becomes facile. However, if the separation distance between the two radicals/radical ions is too large, the geminate characteristic gets lost and consequently MFE cannot be observed. Thus, MFE requires an optimum distance of separation of the radicals/radical ions in order to preserve their spin-correlation and is observed mostly when the partner radicals/radical ions are separated by about 10−20 Å. A confined medium such as micelles,[20] reverse micelles[21] or vesicles, which facilitate the close proximity of the radical or radical ions formed as a result of PET, provides the ideal conditions to obtain appreciable MFE. In the case of drug−protein interaction, the confinement of the radicals or radical ions may be provided by the complex structure of the protein, which may help the radicals or radical ions to remain geminate as well as spin correlated and eventually exhibit substantial MFE. In this context, it is noteworthy that Scaiano et al. has suggested that application of an external MF can act as a cocarcinogen in biological systems as MF-enhanced free-radical attack may weaken the biological response to genotoxic stress and, consequently, promote increased mutagenesis and cancer.[22] The essence of usage of an external MF in the case of drug−protein interaction is thus comprehensible besides its role of serving as a tool in the elucidation of reaction mechanisms.

Acridine-based drugs are often used as photosensitizers in photodynamic therapy (PDT), which is an emerging modality in the treatment of cancer[23−25] as well as some other diseases. Acridine yellow (AY) and cationic proflavin (PF^+) (as depicted in Figure 2a,b respectively) are model photosensitizers in PDT and thus have drawn the interest of researchers.[23,24] PF^+ is known to aggregate above 10^{-4} (M),[26,27] and AY also has a tendency to form aggregates.[28] This property of aggregation may be of significance because the mechanism of PDT involves the localization of the photosensitizers in tumors. PDT is actually based on the concept of preferential accumulation of photosensitizers in the unwanted cells and irradiation with visible light in the presence of oxygen. Additionally, these acridine-based drugs are well-known for their antifungal and antibacterial properties as well as for their interactions with DNA.[29−31] Thus, the study of interactions of AY and PF^+ with exogenous and endogenous drug-delivery vehicles is of utmost importance.

Human serum albumin (HSA), a single polypeptide chain, serves as a potential drug delivery vehicle[32,33] and is the most abundant carrier protein in blood plasma. HSA is composed of 585 amino acid residues and 17 disulfide bridges, and the study of its three-dimensional (3D) crystalline structure reveals that it has three homologous α-helical domains, I, II, and III (I: residues 1−195; II: residues 196−383; III: residues 384−585[34]), each of which has been further classified into subdomains A and B (Figure 2c). Among the six, only two subdomains, viz., subdomains IIA and IIIA (also known as Sudlow's site I and site II, respectively) are capable of binding aromatic and heterocyclic ligands. Subdomain IIA contains the sole tryptophan residue (W214) of HSA, which is the major fluorophore (λ_{em} = 350 nm) of the protein.

Our present work is an endeavor to study the interactions of these two photosensitizers of PDT, viz., AY and PF^+ with the drug delivery vehicle HSA at a pH of 7.4 using conventional spectroscopic methods as well as docking techniques to decipher the binding mechanisms and laser flash photolysis coupled with an external MF to explore PET in drug−protein interaction.

2. Experimental Methods

2.1. Reagents. PF^+ and AY were obtained from Sigma. Fatty acid- and globulin-free HSA was obtained from Fluka. All the solutions were prepared in a 10 mM phosphate buffer of pH 7.4.

2.2. Apparatus. ***2.2.1. Absorption Spectroscopy.*** UV−vis absorption spectra were recorded on a Thermospectronic absorption spectrophotometer (Unicam UV-500) at 298 K. A pair of 1 × 1 cm path length quartz cuvettes was used for absorption experiments. The concentration of the protein was determined spectrophotometrically using the molar extinction coefficient of HSA at 280 nm (ε_{280}) as 36 600 $M^{-1}cm^{-1}$.[35]

2.2.2. Fluorescence Spectroscopy. The steady-state fluorescence measurements were made in a Spex fluoromax-3 spectrofluorimeter using a 1 × 1 cm path length quartz cuvette at 298, 308, 313, and 318 K, and during the steady-state fluorescence measurements the samples were excited at 280 nm. The emission spectra were recorded from 290 to 650 nm. Singlet-state fluorescence lifetime studies were carried out with a time-correlated single-photon-counting (TCSPC) spectrophotometer (Edinburgh,) and during lifetime study the samples were excited at 297 nm. Lifetime was obtained using deconvolution technique, which is based on a convolution integral. The fluorescence of HSA was corrected for inner filter effect owing to absorbance by the two PDT drugs at the excitation and emission wavelengths, using the following equation:[36]

$$F_{corr} = F_{obs} \times \text{antilog}\left[\frac{OD_{ex} + OD_{em}}{2}\right] \quad (1)$$

where F_{corr} and F_{obs} are the corrected and observed fluorescence intensities, respectively, and OD_{ex} and OD_{em} are the absorbances at excitation and emission wavelengths, respectively.

2.2.3. CD Spectroscopy. CD measurements were made on a Jasco-720 automatic recording spectrophotometer using a 0.1 cm path length cuvette. An accumulation of three scans with a scan speed of 20 nm per minute and response time of 2 s was performed to collect data.

2.2.4. Transient Absorption Measurement. Nanosecond flash photolysis setup (Applied Photo Physics) containing a Nd:YAG (Labseries, Model Lab150, Spectraphysics) laser was used for the measurement of transient absorption spectra. The sample was excited at 266 nm (full width at half-maximum (fwhm) = 8 ns) laser light. Transients were monitored through absorption of light from a pulsed xenon lamp (250 W). The photomultiplier (IP28) output was fed into a Tektronix oscilloscope (TDS 3054B, 500 MHz, 5 Gs/s), and the data were transferred to a computer using the TekVISA software. The software Origin 5.0 was used for curve fitting. The solid curves were obtained by connecting the points by using the B-Spline option. The samples were deaerated by passing pure argon gas for 20 min prior to each experiment. No degradation of the samples was observed during the experiment. The MF (0.08 T) effect on the transient spectra was studied by passing direct current through a pair of electromagnetic coils placed inside the sample chamber.

2.3. Methods. ***2.3.1. Calculation of Mean Residual Ellipticity (MRE) and α-Helical Content of Proteins by CD Spectroscopy.*** The results of CD were expressed as MRE (in deg cm^2 $dmol^{-1}$) according to the following equation:[37]

$$\text{MRE} = \frac{\text{observedCD(mdeg)}}{C_p n l \times 10} \quad (2)$$

where C_p is the molar concentration of the protein, n is the number of amino acid residues, and l is the path length. For HSA, $n = 585$,[37] and we used cuvettes with $l = 0.1$ cm. The α-helical content of free and bound protein was eventually evaluated from the MRE value at 208 nm using the formula[37]

$$\alpha\text{-helix}\% = \left[\frac{-\text{MRE}_{208} - 4000}{33000 - 4000}\right] \times 100 \quad (3)$$

where, MRE_{208} is the observed MRE value at 208 nm, 4000 is the MRE of β-form and random coil conformation at 208 nm, and 33000 is the MRE value of a pure α-helix at 208 nm.

2.3.2. FRET Calculation. Förster's theory of energy transfer was used to evaluate the distance between the fluorophore in the protein and the drug. In this context, efficiency of energy transfer E is given by

$$E = 1 - \left(\frac{F}{F_0}\right) = \frac{{R_0}^6}{{R_0}^6 + r^6} \quad (4)$$

where r is the distance between the donor and acceptor and R_0 is the critical energy transfer distance, at which 50% of the excitation energy is transferred to the acceptor and is given by the following equation:

$${R_0}^6 = 8.79 \times 10^{-25} \kappa^2 n^{-4} J \phi \quad (5)$$

In eq 5, κ^2 is the spatial orientation factor describing the relative orientation in space of the transition dipoles of the donor and acceptor, n is the refractive index of the medium, ϕ is the fluorescence quantum yield of the donor in the absence of the acceptor, and J is the overlap integral of the fluorescence emission spectrum of the donor and the absorption spectrum of the acceptor. The value of J is given by the equation

$$J = \frac{\left(\sum F(\lambda)\varepsilon_A(\lambda)\lambda^4 \Delta\lambda\right)}{\left(\sum F(\lambda)\Delta\lambda\right)} \quad (6)$$

where, $F(\lambda)$ is the fluorescence intensity of the fluorescent donor at wavelength λ, and $\varepsilon(\lambda)$ is the molar absorption coefficient at wavelength λ. Under the experimental conditions, $k^2 = 2/3$, $n = 1.336$,[36] and $\phi = 0.118$ for HSA.[38] Values of E and J were obtained experimentally.

Rate of energy transfer (k_{ET}) depends on the lifetime of the donor molecule and is given by[36]

$$k_{ET} = \frac{1}{\tau_D}\left(\frac{R_0}{r}\right)^6 \quad (7)$$

where τ_D is the lifetime of the donor molecule in the absence of the acceptor moiety.

2.3.3. Calculation of Binding Constant (K) and Number of Binding Sites (n). In order to determine the binding constant (K) and the number of binding sites (n), the following equation was employed:[1]

$$\log\left(\frac{F_0 - F}{F}\right) = \log K + n \log[Q] \tag{8}$$

where, F_0 and F are the fluorescence intensities in the absence and presence of quencher, and $[Q]$ is the concentration of quencher. $\log(F_0 - F)/F$ was plotted against $\log[Q]$, and the values of K and n were obtained from the intercept and slope, respectively.

2.3.4. Calculation of the Thermodynamic Parameters. The van't Hoff and Gibbs−Helmholtz equations were used for determination of the thermodynamic parameters:

$$\ln K = -\left(\frac{\Delta H^\circ}{RT}\right) + \left(\frac{\Delta S^\circ}{R}\right) \tag{9}$$

and

$$\Delta G^\circ = \Delta H^\circ - T\Delta S^\circ \tag{10}$$

$\ln K$ was plotted against $1/T$, and ΔH° and ΔS° were obtained from the slope and the intercept of the plot, respectively, and then the values of ΔG° at different temperatures were determined by making use of eq 10.

2.4. Molecular Docking Studies. The crystal structure of HSA was obtained from the Protein Data Bank[39] (PDB entry 1AO6) and was used for the docking studies. Energy-minimized structures of AY and PF^+ were generated in Sybyl 6.92 (Tripos Inc., St. Louis, MO, USA) with the help of Tripos force field using Gasteiger−Hückel charges with 1000 iterations by the Powell method. The FlexX program available as part of the Sybyl suite was used for docking of AY and PF^+ to HSA. PyMol[40] was used to visualize the docked conformations.

The accessible surface area (ASA) of HSA (uncomplexed) and its docked complex with AY and PF^+ were calculated using NACCESS.[41] The protein−ligand structure corresponding to the minimum score as obtained from the FlexX analysis was chosen, and composite coordinates of the complex were generated. The change in ASA for residue was calculated using $\Delta ASA = ASA_{HSA} - ASA_{HSA\text{-ligand}}$.

3. Results and Discussion

3.1. UV−Vis Absorption Spectroscopy. To gain insight into the mode of binding of the two novel acridine derivatives with HSA, UV−vis absorption spectroscopy is used. Both of the acridine-based drugs have significant absorptions in the wavelength range of 320−500 nm, but the protein has no absorption in this region, as evident from Figure 3a. The calculated amount of the drug along with the buffer solution is used as the reference solution. The absorption spectrum is monitored by gradually increasing the concentration of HSA to the calculated amount of drugs. Emergence of peaks is observed in both cases, with λ_{max} at 445 and 393 nm for PF^+ and AY, respectively (as shown in Figure 3b,c), and their intensity increased with increase in concentration of HSA. As the contribution of absorbance of the drugs has already been eliminated by using the calculated amount of drug along with the buffer solution as the reference solution as well as the fact that HSA intrinsically has no absorption in the in the region 320−500 nm, the advent of the new peak may be attributed to ground-state complexes formed between the drugs and the protein. Therefore, the use of this method removes the contribution of absorbance of the drugs and shows the formation of the ground-state complexes, even though these complexes have absorption maxima in the region characteristic of that of the two acridine derivatives (380−500 nm). Such a method has already been used earlier to confirm the occurrence of the process of ground-state complex formation.[4] Thus, absorption spectroscopy reveals the formation of ground-state complexes between the acridine derivatives and HSA.

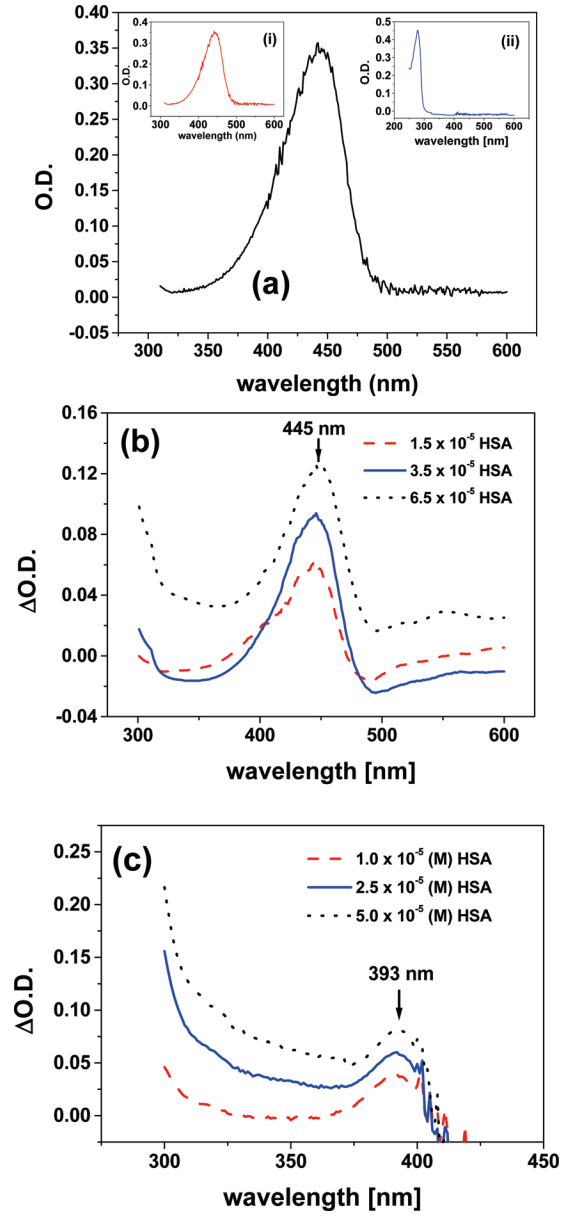

Figure 3. (a) Absorption spectrum of AY; $[AY] = 1 \times 10^{-5}$ (M). Insets show (i) absorption spectrum of PF^+, $[PF^+] = 1 \times 10^{-5}$ (M), and (ii) absorption spectrum of 1.25×10^{-5} (M) HSA showing λ_{max} at 280 nm and no absorption in the range 310−600 nm. (b) Absorption spectrum showing the formation of the PF^+−HSA ground-state complex. $[PF^+] = 2.0 \times 10^{-5}$ (M); [HSA] ranges from 1.5×10^{-5} (M) to 6.5×10^{-5} (M). (c) Absorption spectrum showing the formation of the AY−HSA ground-state complex. $[AY] = 2.0 \times 10^{-5}$ (M); [HSA] ranges from 1.0×10^{-5} (M) to 5.0×10^{-5} (M).

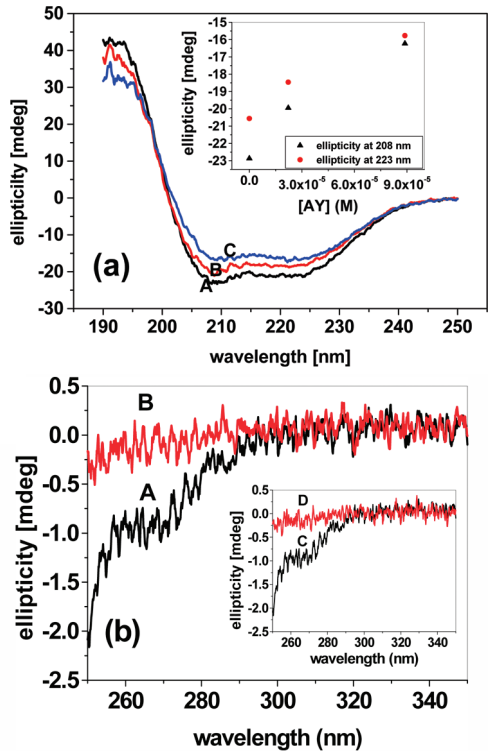

Figure 4. (a) Far-UV CD spectra showing the variation of ellipticity at 208 and 223 nm on addition of AY to HSA. [HSA] = 1.5×10^{-6} (M), and [AY] are (A) 0, (B) 2×10^{-5} (M), and (C) 8×10^{-5} (M). Inset shows the variation of ellipticity at 208 nm (▲) and 223 nm (●) as a function of concentration of AY. (b) Near-UV CD spectra of (A) 1.5×10^{-6} (M) HSA and (B) 1.5×10^{-6} (M) HSA + 2×10^{-5} (M) AY. The inset shows the near-UV CD spectra of (C) 1.5×10^{-6} (M) HSA and (D) 1.5×10^{-6} (M) HSA + 2×10^{-5} (M) PF^+.

Now, free AY and PF^+ show absorption maxima around 440 nm. The characteristic peak of the ground-state complex formed between HSA and AY emerges around 393 nm, which is blue-shifted with respect to free AY (440 nm), thus implying the prevalence of hydrophobic interaction. However, the characteristic peak of the ground-state complex formed between HSA and PF^+ appears around 445 nm, which is slightly red-shifted with respect to that of free PF^+. Literature survey suggests that hydrogen bond formation is associated with red shift of the absorption spectrum.[42−44] Thus, the emergence of the red-shifted peak indicates that the complex formed between HSA and PF^+ possibly involves hydrogen bonding.

3.2. CD Studies. CD, a very sensitive technique often employed in the study of drug−protein interaction, is used to monitor the changes in secondary and tertiary structures of the model protein resulting from its interaction with the derivatives of acridine. Native HSA is found to show two negative bands in the far-UV region (190−250 nm) at 208 and 223 nm, a typical characteristic of an α-helical protein. On addition of PF^+ solution, there is no appreciable change in the far-UV CD spectrum of HSA, indicating that PF^+ induces no substantial change in the secondary structure of the protein. On the other hand, addition of AY solution leads to decrease in the intensity of both of the negative bands (at 208 and 223 nm) as depicted in Figure 4a, which is indicative of the change in conformation of the protein on binding with the ligands. The α-helix content of HSA in the presence and absence of AY is calculated using eqs 2 and 3 and is summarized in Table 1. The quantitative analysis of CD results shows that α-helix% of HSA changes from 79.18 to 52.18, signifying a loss of α-helix content on binding with AY. Increase in the magnitude of MRE and

TABLE 1: Variation in α-helix% of HSA with Increase in AY Concentration

[HSA] (M)	[AY] (M)	α-helix%
1.5×10^{-6}	0	79.18
1.5×10^{-6}	2.0×10^{-5}	63.13
1.5×10^{-6}	8.0×10^{-5}	52.18

α-helix% is indicative of stabilization of a protein upon binding with drug.[1] So, in the case of the AY−HSA system, far-UV CD results imply that the helical structure of the protein is somewhat destabilized on binding with AY. However, there is an appreciable change in the near-UV CD spectra (250−350 nm) when both the acridine derivatives are added to native HSA (as shown in Figure 4b), implying that ligand binding perturbs the tertiary structure of the protein and imparts significant conformational changes in the regions of aromatic amino acid residues and disulfide bonds. Therefore, AY brings about changes in both secondary as well as tertiary structures of HSA, while PF^+ imparts change only in the tertiary structure. Actually, subtle differences in conformation do not produce a detectable difference in far-UV CD, but may produce a difference in near-UV CD. In fact, for a ligand binding process to be detectable in the far-UV CD spectrum, a considerable fraction of the peptide groups must be perturbed, while, if the process affects the conformation or environment around an aromatic side chain or disulfide bridge, that contributes significantly to the near-UV CD and it can be detected. The presence of two additional methyl groups in AY makes the drug more hydrophobic compared to PF^+ and can effectively perturb the hydrophobic pockets of the protein more efficiently than PF^+, thus eventually imparting a more prominent change in the structure of HSA. This differential behavior of the two drugs is later substantiated by the ASA calculation of the docking studies. We have also performed CD of PF^+ and AY to check whether binding of HSA imparts any conformational change to the ligand, but no protein-induced CD changes are observed.

3.3. Fluorescence Spectroscopy. HSA displays an intrinsic emission maximum around 350 nm, while the two acridine-based drugs fluoresce around 508 nm. The intrinsic fluorescence of HSA is quenched on addition of PF^+ as well as AY solution accompanied by simultaneous enhancement of the fluorescence of the drugs (as shown in Figure 5a,b). Enhancement of fluorescence of drugs at the cost of fluorescence of HSA is indicative of the fact that there exists some sort of interaction between HSA and the two ligands. In both cases, isoemissive points are obtained around 455 nm. Another related observation, which is noteworthy in this case, is that with increase in concentration of the drugs there is a slight blue shift in the λ_{max} of HSA, implying that the environment around the fluorophore in the protein (Trp 214) becomes hydrophobic on addition of the ligands. The shift is more prominent for AY compared to PF^+ probably because of the more hydrophobic nature of AY compared to PF^+ owing to the presence of two additional methyl groups.

To determine the mechanism of fluorescence quenching, fluorescence data is analyzed using the Stern−Volmer equation:

$$\frac{F_0}{F} = 1 + K_{SV}[Q] \qquad (11)$$

where F_0 and F are the fluorescence intensities of HSA in the absence and presence of quencher, respectively, K_{SV} is the Stern−Volmer constant, and $[Q]$ is the concentration of the

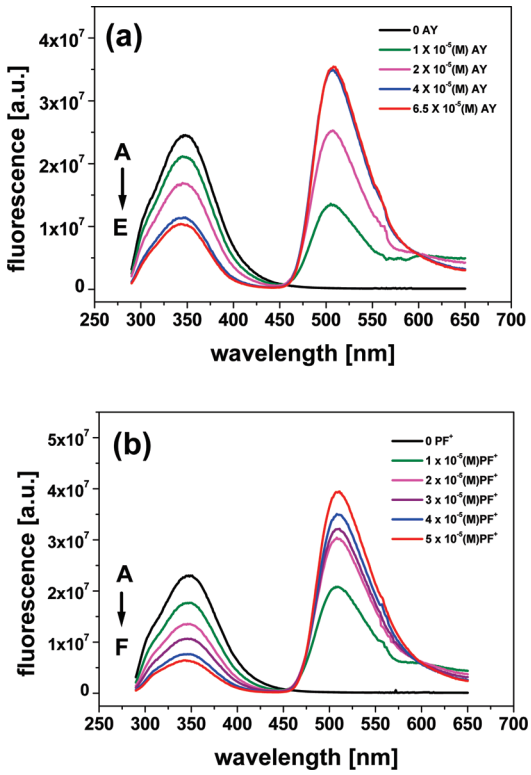

Figure 5. (a) Fluorescence spectra showing quenching of intrinsic fluorescence of HSA with increase in AY concentration accompanied by enhancement of fluorescence of AY. λ_{ex} = 280 nm. [HSA] = 1.5 × 10^{-5} (M); [AY] = (A) 0, (B) 1 × 10^{-5} (M), (C) 2 × 10^{-5} (M), (D) 4 × 10^{-5} (M), and (E) 6.5 × 10^{-5} (M). (b) Fluorescence spectra showing quenching of intrinsic fluorescence of HSA with increase in PF^+ concentration accompanied by enhancement of fluorescence of PF^+. λ_{ex} = 280 nm. [HSA] = 1.5 × 10^{-5} (M); [PF^+] = (A) 0, (B) 1 × 10^{-5} (M), (C) 2 × 10^{-5} (M), (D) 3 × 10^{-5} (M), (E) 4 × 10^{-5} (M), and (F) 5 × 10^{-5} (M).

quencher. As evident from Figure 6a,b, both of the Stern−Volmer plots of quenching of steady-state fluorescence of HSA show positive deviation from linearity. In general, positive deviation from linearity of a Stern−Volmer plot of quenching of steady-state fluorescence occurs primarily when a combination of static and dynamic quenching takes place.[36] The fact that the mechanism of static quenching is present for both AY−HSA and PF^+−HSA systems has already been proved by ground-state complex formation in both cases. Now, time-resolved fluorescence study is carried out to verify the possibility of dynamic quenching. The fluorescence lifetime of HSA decreases significantly on addition of both ligands (as shown in Table 2), thus showing the prevalence of the mechanism of dynamic quenching for both cases. Tryptophan exhibits multiexponential decay, and its average lifetime has been used in order to obtain a quantitative picture. As time-resolved fluorescence data accounts only for dynamic quenching, the lifetime Stern−Volmer plot is expected to be linear as depicted in the insets of Figure 6a,b. Repetitive fluorescence lifetime experiments have reproduced the same results, thus confirming the occurrence of dynamic quenching. Thus, in the case of both AY−HSA and PF^+−HSA systems, the cause of positive deviation of Stern−Volmer plot can be attributed to the simultaneous occurrence of static and dynamic quenching processes. Such an upward curvature of the Stern−Volmer plot has also been observed while studying the interaction of chlorin derivatives with HSA, which has been attributed to the co-occurrence of more than one mechanism of quenching.[2]

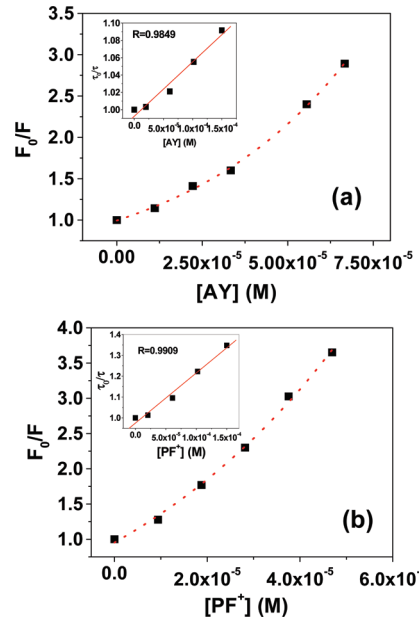

Figure 6. (a) Stern−Volmer plot of quenching of steady-state fluorescence of HSA by AY. [HSA] = 1.5 × 10^{-5} (M); [AY] ranges from 0 to 6.5 × 10^{-5} (M). Inset shows time-resolved Stern−Volmer plots for quenching of fluorescence of HSA by AY. [HSA] = 1.5 × 10^{-5} (M); [AY] ranges from 0 to 1.5 × 10^{-4} (M). (b) Stern−Volmer plot of quenching of steady-state fluorescence of HSA by PF^+. [HSA] = 1.5 × 10^{-5} (M); [PF^+] ranges from 0 to 5 × 10^{-5} (M). Inset shows time-resolved Stern−Volmer plots for quenching of fluorescence of HSA by PF^+. [HSA] = 1.5 × 10^{-5} (M); [PF^+] ranges from 0 to 1.5 × 10^{-4} (M).

TABLE 2: Variation of Lifetime (τ) of HSA with Increase in Concentration of PF^+ and AY

[HSA] (M)	concentration of ligand (M)	τ (ns) on addition of PF^+	τ (ns) on addition of AY
1.5 × 10^{-5}	0	6.32	6.32
1.5 × 10^{-5}	2.0 × 10^{-5}	6.24	6.30
1.5 × 10^{-5}	6.0 × 10^{-5}	5.77	6.19
1.5 × 10^{-5}	1.0 × 10^{-4}	5.17	5.99
1.5 × 10^{-5}	1.5 × 10^{-4}	4.69	5.79

In order to evaluate K_{SV} in both the cases, we have considered the range within which the Stern−Volmer plots show linearity,[4] and eventually the quenching rate constant, k_q, is evaluated by using the following equation:

$$K_{SV} = k_q \tau_0 \tag{12}$$

where τ_0 is the lifetime of HSA in the absence of the quencher. The values of K_{SV} are 1.86 × 10^4 M^{-1} and 4.68 × 10^4 M^{-1}, and finally, the k_q values so obtained are 2.99 × 10^{12} M^{-1} s^{-1} and 7.59 × 10^{12} M^{-1} s^{-1} for AY−HSA and PF^+−HSA interactions, respectively. It is well-known that the upper limit of the value of k_q for diffusion-controlled phenomenon is of the order of 10^{10}.[45] Therefore, the exceptionally high values of k_q for AY−HSA and PF^+−HSA interactions are indicative of the energy transfer process from the HSA to the ligands.[4,46,47] Another indication of energy transfer from the protein to the ligands is that there is enhancement in the fluorescence of the ligands at the cost of the fluorescence of HSA along with the formation of an isoemissive point, which has already been discussed earlier in this section.

The required condition of spectral overlap for FRET, i.e., overlap of the absorption spectrum of the acceptor and the

TABLE 3: Summary of the Values of Efficiency of Energy Transfer *E*, Spectral Overlap Integral *J*, Critical Energy Transfer Distance R_0, the Distance between the Fluorophore and the Ligand *r*, and the Rate of Energy Transfer k_{ET} for AY−HSA and PF^+−HSA Systems

system	*E*	*J* ($M^{-1}cm^3$)	R_0 (Å)	*r* (Å)	k_{ET} (s^{-1})
AY−HSA	0.243	9.77×10^{-15}	24.42	29.51	5.08×10^7
PF^+−HSA	0.324	1.03×10^{-14}	24.62	27.83	7.58×10^7

fluorescence spectrum of the donor, is fulfilled for both AY−HSA and PF^+−HSA systems. Now, the decrease in fluorescence intensity of HSA on addition of PF^+ and AY may be either due to direct energy transfer from the singlet-excited state of HSA (Trp to be precise) to the acridine derivatives or due to inner filter effect owing to absorbance by both the PDT drugs in the absorption and emission wavelengths. Fluorescence lifetime measurement of HSA in the presence and absence of the ligands can be a potent tool to verify the actual cause of fluorescence quenching. As evident from Table 2, it is found that the lifetime of 15 μM HSA decreases on gradual addition of the PDT drugs, thus suggesting that quenching of intrinsic fluorescence of HSA by the acridine derivatives is not due to inner filter effect, but because of energy transfer. Priyadarsini and co-workers have reported similar observations while studying the interaction of curcumin with HSA.[48] Förster's theory of nonradiative energy transfer is employed to calculate the efficiency of energy transfer (*E*) and the distance between ligands and tryptophan residue (Trp 214) in HSA. The efficiency of energy transfer signifies the fraction of photons absorbed by the donor that are transferred to the acceptor.[36] Thus, the smaller the donor−acceptor distance, the higher the value of energy transfer efficiency. This is also evident from eq 4. By using the required equations, the values of critical energy transfer distance (R_0) and the distance between the donor and the acceptor (*r*) are evaluated for both systems, and their values are given in Table 3. The values of *r* for AY−HSA and PF^+−HSA systems are found to be 29.51 Å and 27.83 Å, respectively. Similar distances have been reported earlier for drugs that prefer to bind to Sudlow's site I, such as curcumin[48] and silibinin.[49] For both HSA−AY and HSA−PF^+ systems, the average donor−acceptor distance $r < 8$ nm and $0.5R_0 < r < 1.5R_0$, implying that energy transfer occurs from HSA to the acridine derivatives with high probability.[4] The higher value of energy transfer efficiency for the PF^+−HSA system compared to that of the AY−HSA system (as depicted in Table 3) indicates that AY is more distant from Trp 214 compared to PF^+. Both experimentally and theoretically, it is found that the AY−HSA distance is more than the PF^+−HSA distance. The rate of energy transfer is calculated using eq 7, and the values are given in Table 3. It is found that k_{ET} for the PF^+−HSA system is almost 1.5 times higher than that of the AY−HSA system.

The values of binding constant (*K*) and the number of binding site (*n*) for both HSA−AY and HSA−PF^+ have been evaluated by making use of the fluorescence data and eq 8 as shown in Table 4. Fluorescence study at four different temperatures, viz., 298, 308, 313, and 318 K, also helps to evaluate the thermodynamic parameters necessary for the determination of interacting forces in the drug−protein interaction.[50] The forces involved in drug−protein interaction are primarily four types, viz., electrostatic forces, hydrophobic forces, van der Waals interactions, and hydrogen bonding. Ross and Subramanian (1981) characterized the signs and magnitudes of the thermodynamic parameters with various individual kinds of forces involved in drug−protein interaction. The thermodynamic parameters obtained by exploiting the fluorescence data and making use of eqs 9 and 10 for both the systems are depicted in Table 4. Interestingly, Table 4 suggests that at any particular temperature, the binding constant for the PF^+−HSA system is more than that of the AY−HSA system. Furthermore, for both PF^+−HSA as well as AY−HSA systems, the value of binding constant decreases with rise in temperature probably because the complex formed loses its stability at higher temperature; but the extent of decrease in binding constant is less for the PF^+−HSA system compared to the AY−HSA system. The findings of the docking study substantiate these interesting observations, which are discussed later in this article.

TABLE 4: Determination of Binding Constants *K*, Number of Binding Sites *n*, and the Thermodynamic Parameters for Both AY−HSA and PF^+−HSA Systems at Different Temperatures

temp (K)	drug	*n*	log *K*	*K* (M^{-1})	$\Delta G°$ kJ mol^{-1}	$\Delta H°$ kJ mol^{-1}	$\Delta S°$ J mol^{-1} K^{-1}
298	AY	1.44	6.275	1.88×10^6	−35.92	−33.80	7.11
	PF^+	1.41	6.518	3.29×10^6	−37.29	−41.63	−14.54
308	AY	1.33	6.144	1.39×10^6	−35.99	−33.80	7.11
	PF^+	1.38	6.329	2.13×10^6	−37.15	−41.63	−14.54
313	AY	1.31	6.010	1.02×10^6	−36.03	−33.80	7.11
	PF^+	1.38	6.184	1.53×10^6	−37.08	−41.63	−14.54
318	AY	1.29	5.901	0.79×10^6	−36.06	−33.80	7.11
	PF^+	1.39	6.058	1.14×10^6	−37.01	−41.63	−14.54

From the signs of the thermodynamic parameters, the nature of forces involved in the drug−protein interaction may be predicted. For both HSA−AY and HSA−PF^+ systems, $\Delta G°$ is negative at all temperatures, implying the reactions are spontaneous. Table 4 shows that $\Delta H°$ is negative for both HSA−AY and HSA−PF^+ systems, indicating that the binding interactions may have considerable contributions from van der Waal's forces and hydrogen bonding interactions. A positive value of $\Delta S°$ for HSA−AY interaction signifies that the interactive forces may involve ionic interactions as well as hydrophobic interactions. In the case of the HSA−PF^+ system, a negative value of $\Delta S°$ indicates that van der Waal's forces and hydrogen bonding are the key forces of association. Thus, taking into account the signs of all the thermodynamic parameters, it may be suggested that for HSA−PF^+ interaction the major interacting forces are van der Waal's forces and hydrogen bonding, whereas for HSA−AY interaction all four forces have significant contributions. The difference in the binding interaction for the two systems may be attributed to a number of factors, viz., the presence of additional methyl groups in AY making the drug relatively hydrophobic and also the interacting residues of the protein. The role of the second factor in determining the nature of the interacting force can be appreciated from the results of docking studies.

3.4. Laser Flash Photolysis and MFE. In order to monitor the interaction of the two acridine derivatives with HSA in the excited state, laser flash photolysis coupled with an external MF (MF = 0.08 T) is employed. Literature survey suggests that the transient absorption spectrum of $TrpH^{\bullet+}$ shows peaks around 350[51] and 560[52] nm, and that of $Trp^{\bullet}$ shows a peak at 520 nm.[53] From our earlier work, we have observed that the transient absorption spectrum of $PF^{\bullet}$ shows a peak around 400 nm along with a weak peak around 520 nm, and $PFH^{\bullet+}$ shows a peak at 550 nm.[54,55] Figure 7a shows the transient absorption spectra of HSA (1.5×10^{-5} M), HSA (1.5×10^{-5} M) + PF^+ (8×10^{-6} M), and HSA (1.5×10^{-5} M) + PF^+ (1.6×10^{-5} M) in phosphate buffer pH 7.4 at 0.1 μs after the laser flash at 266 nm. It is observed that, on addition of PF^+ to HSA, the absorbance around 350, 380, 520, 550, and 560 nm increases

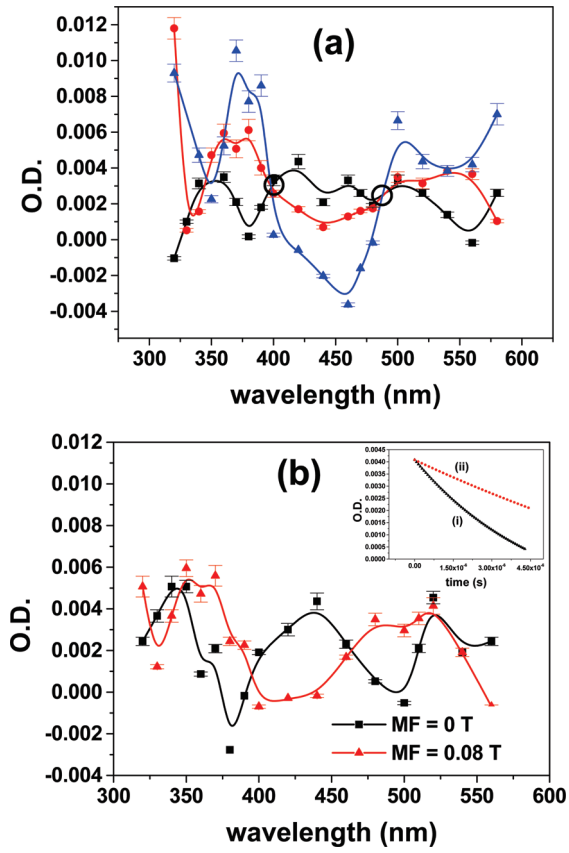

Figure 7. (a) Transient absorption spectra of 1.5×10^{-5} (M) HSA (■), 1.5×10^{-5} (M) HSA + 8×10^{-6} (M) PF^+ (●), and 1.5×10^{-5} (M) HSA + 1.5×10^{-5} (M) PF^+ (▲) in phosphate buffer at a delay of 0.1 μs after the laser flash showing isosbestic points at 400 and 487 nm. (b) Transient absorption spectra of 1.5×10^{-5} (M) HSA + 2×10^{-6} (M) PF^+ in absence (■) and presence (▲) of magnetic field in phosphate buffer at a delay of 0.1 μs after the laser flash. Inset shows the decay profile of 1.5×10^{-5} (M) HSA + 2×10^{-6} (M) PF^+ in phosphate buffer in (i) absence and (ii) presence of magnetic field at 350 nm, which is the signature of $TrpH^{\bullet+}$.

significantly accompanied by the formation of two isosbestic points at 398 and 487 nm. The increase in absorbance at 350 and 560 can be attributed to $TrpH^{\bullet+}$, and that at 550 and 520 can be unambiguously assigned to $PFH^{\bullet+}$ and $Trp^{\bullet}$. Now, the pertinent question that arises here is how do $PFH^{\bullet+}$ and $Trp^{\bullet}$ arise? Earlier work shows that the process of random proton transfer is a common phenomenon in the case of tryptophan residues in proteins.[51,56] In the case of HSA-PF^+ system, such a phenomenon of proton transfer is present, which can be represented as

$$^3PF^{\bullet} + TrpH^{\bullet+} \xrightarrow{H^+\text{transfer}} PFH^{\bullet+} + Trp^{\bullet}$$

Thus, it may be proposed that PET takes place from tryptophan residue of the protein to PF^+. As PF^+ bears a unipositive charge at pH 7.4,[57] in the due course of PET, PF^+ yields a radical ($PF^{\bullet}$) instead of a radical anion ($PF^{\bullet-}$), which eventually produces the spin-correlated geminate pair ($TrpH^{\bullet+}$ $PF^{\bullet}$) that undergoes proton transfer within the geminate cage to yield spin-correlated ($Trp^{\bullet}$ $PFH^{\bullet+}$).

The peak at 380 nm may be assigned to the HSA−PF^+ complex,which is pumped from the ground-state to singlet excited by 266 nm laser, undergoes ISC to the triplet state, and is probed by Xe to higher triplet states. Transient absorption of the complex shows a characteristic peak at 380 nm.

$$HSA + PF^+ \rightarrow {}^1(HSA{-}PF^+)$$

$$^1(HSA{-}PF^+) \xrightarrow{h\nu} {}^1(HSA{-}PF^+)^*$$

$$^1(HSA{-}PF^+)^* \xrightarrow{ISC} {}^3(HSA{-}PF^+)^*$$

Figure 7b shows the transient absorption spectra of HSA (1.5×10^{-5} M) + PF^+ (2×10^{-6} M) in the presence and absence of MF in phosphate buffer at a delay of 0.1 μs after the laser flash. In the presence of an MF, there is considerable enhancement of the absorbance around 350, 380, 400, 520, 550, and 560 nm. Increase in absorbance at 350, 400, and 560 nm is due to MFE exhibited by the spin-correlated geminate pair ($PF^{\bullet}$ $TrpH^{\bullet+}$), which arises out of the coupling of its spin and diffusion dynamics. The inset of Figure 7b shows the decay profile of 1.5×10^{-5} (M) HSA + 2×10^{-6} (M) PF^+ in phosphate buffer in (i) the absence and (ii) the presence of MF at 350 nm, which is the signature of $TrpH^{\bullet+}$. Marked increase in absorbance at 520 and 550 nm arises from sufficient coupling of spin and diffusion dynamics of the spin correlated geminate pair ($PFH^{\bullet+}$ $Trp^{\bullet}$), which is a product of proton transfer within the geminate cage of ($PF^{\bullet}$ $TrpH^{\bullet+}$). As geminate character and spin correlation of the radicals/radical ions are primary conditions of MFE, it is proved that the process of proton transfer in this case is ultrafast and takes place in the geminate cage within the short period of spin-flipping. The radicals/radical ions, which are initially formed in the triplet state, diffuse to an optimum distance in the medium, and, when an external MF is applied, there is reduction of ISC leading to an enhancement in the triplet yield of the respective radicals/radical ions. This explains the increase in absorbance at 350, 400, 520, 550, and 560 nm. Increased yield of the radicals/radical ions on application of MF also confirms that their parent spin state is triplet. Increase in absorbance at 380 nm on application of MF may be attributed to partial charge separation in the complex in the triplet state, eventually producing spin-correlated radicals/radical ions, which exhibit MFE.

The proposed reaction mechanism is as follows:

$$^1PF^+ \xrightarrow{h\nu} {}^1(PF^+)^* \xrightarrow{ISC} {}^3(PF^+)^*$$

$$^3(PF^+)^* + TrpH \rightarrow {}^3(PF^{\bullet}\ TrpH^{\bullet+}) \leftrightarrow \text{proton transfer} \leftrightarrow {}^3(PFH^{\bullet+}\ Trp^{\bullet})$$

$$^3(PF^{\bullet}\ TrpH^{\bullet+}) \underset{HFI}{\overset{MFE}{\longleftrightarrow}} {}^1(PF^{\bullet}\ TrpH^{\bullet+})$$

$$^3(PFH^{\bullet+}\ Trp^{\bullet}) \underset{HFI}{\overset{MFE}{\longleftrightarrow}} {}^1(PFH^{\bullet+}\ Trp^{\bullet})$$

Although PET takes place from tryptophan to PF^+, the enhancement in absorbance at 400 nm (signature of $PF^{\bullet}$) and

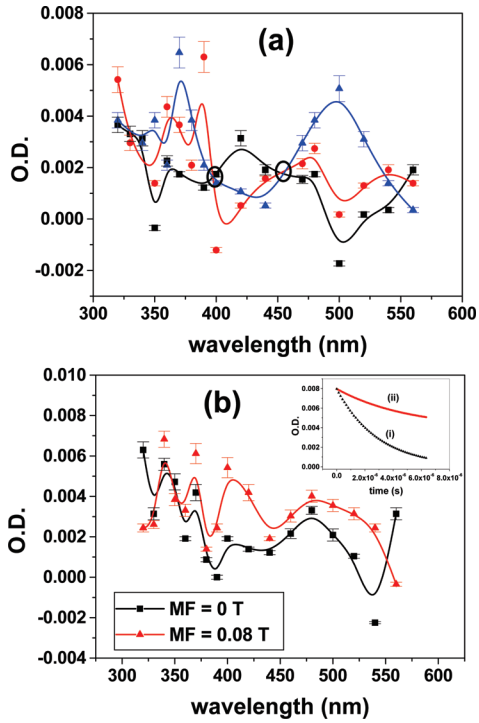

Figure 8. (a) Transient absorption spectra of 1.5×10^{-5} (M) HSA (■), 1.5×10^{-5} (M) HSA + 3×10^{-6} (M) AY (●), and 1.5×10^{-5} (M) HSA + 8×10^{-6} (M) AY (▲) in phosphate buffer at a delay of 0.6 μs after the laser flash showing isosbestic points at 396 and 454 nm. (b) Transient absorption spectra of 1.5×10^{-5} (M) HSA + 3×10^{-6} (M) AY in absence (■) and presence (▲) of magnetic field in phosphate buffer at a delay of 0.6 μs after the laser flash. Inset shows the decay profile of 1.5×10^{-5} (M) HSA + 3×10^{-6} (M) AY in phosphate buffer in (i) absence and (ii) presence of magnetic field at 350 nm, which is the signature of $TrpH^{\bullet+}$.

560 nm (signature of $TrpH^{\bullet+}$) is not appreciable. This may be attributed to very fast proton transfer within the geminate cage $^3(PF^{\bullet}\ TrpH^{\bullet+})$ to yield $^3(PFH^{\bullet+}\ Trp^{\bullet})$ in the case of the PF^+−HSA system. Thus the peaks corresponding to the escaped products from the geminate cage $^3(PF^{\bullet}\ TrpH^{\bullet+})$, $PF^{\bullet}$ (400 nm) and $TrpH^{\bullet+}$ (560 nm), do not show appreciable enhancement in the presence of MF; instead, there is significant enhancement in the peak corresponding to those originated from $^3(PFH^{\bullet+}\ Trp^{\bullet})$, i.e., $PFH^{\bullet+}$ and $Trp^{\bullet}$. However, the peak at 350 nm corresponding to $TrpH^{\bullet+}$ shows remarkable enhancement in the presence of MF due to the overlap with neighboring MFE at 380 nm corresponding to the PF^+−HSA complex. As the peak centered around 380 nm owing to the complex is large, it seems that there is a considerable enhancement at 350 nm. Moreover, the contribution in the increase in absorbance in the presence of MF at 400 nm from $PF^{\bullet}$ becomes insignificant in comparison to that obtained from the complex at 380 nm.

Similar observations are recorded for the AY−HSA system. With increase in concentration of AY, absorbance around 350, 370, 400, and 520 nm increases, accompanied by the formation of two isosbestic points at 396 and 454 nm (as shown in Figure 8a). Earlier we characterized the peak for $AY^{\bullet-}$ at 400 nm in the transient absorption spectrum.[58] Increase in absorbance at 350, 400, and 520 nm implies the formation of $TrpH^{\bullet+}$, $AY^{\bullet-}$, and $Trp^{\bullet}$, respectively, implying that the processes of PET as well as proton transfer are present in the AY−HSA system. The peak around 370 nm can be assigned to the HSA−AY ground-state complex, which is pumped by laser to a higher singlet state, undergoes ISC, and eventually triplet−triplet transition.

TABLE 5: Decay Rate Constant (k_f) and Relative Radical Escape Yield (γ) of $TrpH^{\bullet+}$, $PF^{\bullet}$, and $AY^{\bullet-}$ in the Absence and Presence of MF

PF^+−HSA system			
wavelength	MF (T)	decay rate constant k_f (s^{-1})	γ
350 nm ($TrpH^{\bullet+}$)	0	2.04×10^5	1.00[a]
	0.08	0.52×10^5	1.63
400 nm ($PF^{\bullet}$)	0	1.79×10^5	1.00[a]
	0.08	0.79×10^5	1.50
AY−HSA system			
wavelength	MF (T)	decay rate constant k_f (s^{-1})	γ
350 nm ($TrpH^{\bullet+}$)	0	3.44×10^5	1.00[a]
	0.08	1.97×10^5	1.65
400 nm ($AY^{\bullet-}$)	0	2.63×10^5	1.00[a]
	0.08	0.38×10^5	1.20

[a] Arbitrarily taken.

The occurrence of PET as well as the original spin state of the precursors of PET in the AY−HSA system are confirmed by the application of an external MF, which leads to prominent increase in absorbance at 350, 370, 400, and 520 nm, as shown in Figure 8b. Increases in absorbance at 350, 400, and 520 are obvious because the concentration of a free radical as well as a radical cation will invariably be affected by the presence of MF. The decay profile of 1.5×10^{-5} (M) HSA + 3×10^{-6} (M) AY at 350 nm in the presence and absence of MF is depicted in the inset of Figure 8b. Interestingly, the peak at 370 nm also shows prominent MFE. This may be because partial charge separation takes place in the complex in the triplet state, thus giving rise to spin-correlated radicals/radical ions, which thereby exhibit MFE, similar to the PF^+−HSA system. The mechanism of reaction pathways in the AY−HSA system is akin to that of the PF^+−HSA system.

In the presence of MF, the decay of the RIP is expected to be biexponential, i.e., the following equation is obeyed for the change in absorbance with time $A(t)$:

$$A(t) = I_f \exp(-k_f t) + I_s \exp(-k_s t) \qquad (13)$$

where k_f and k_s are the rate constants for the fast and slow components of the decay profiles, respectively.[59] The fast component corresponds to the decay of geminate RIPs and the slower one corresponds to that of the escaped radicals. The k_f values obtained from the biexponential fitting of the decay profiles of $TrpH^{\bullet+}$, $PF^{\bullet}$, and $AY^{\bullet-}$ in the absence and presence of MF is given in Table 5. It is observed that, on application of an external MF, the decay rate decreases, and, correspondingly, the escape yield increases. This also implies that RIPs are generated in the triplet state. On application of a MF, the conversion of the triplet RIP to the singlet RIP is retarded, and, consequently, the decay rates become slower, and escape yield is enhanced.

Thus, use of the external MF ensures that the process of PET is prevalent in both PF^+−HSA and AY−HSA systems and that the initial spin state of the precursors of PET is triplet, which would otherwise go unnoticed if only steady-state observations were taken into account. As discussed in the introduction, a confined medium provides the ideal condition to obtain MFE. However, in the present systems, MFE is obtained in homogeneous medium, which is a rare phenomenon. Actually, a pseudoconfined medium is created by the complex structure of the protein that helps to sustain the optimum conditions required

TABLE 6: Changes in the ASA (ΔASA) in Å^2 of Interacting Residues of HSA (Uncomplexed) and Its Complexes with (a) AY and (b) PF$^+$

(a)

residues	domain	ASA_{HSA}	ASA_{HSA-AY}	ΔASA
Arg 209	IIA-h2	129.8	108.15	21.65
Ala 210	IIA-h2	25.81	25.6	0.21
Lys 212	IIA-h2	71.13	34.49	36.64
Ala 213	IIA-h2	35.05	11.74	23.31
Val 216	IIA-h2	15.02	0	15.02
Phe 228	IIA-h3	39.75	27.52	12.23
Ser 232	IIA-h3	37.04	7.91	29.13
Val 235	IIA-h3	4.93	0	4.93
Thr 236	IIA-h3	75.7	63.41	12.29
Asp 324	IIB-h2	76.96	46.55	30.41
Val 325	IIB-h2	84.55	71.5	13.05
Leu 327	IIB-h2	19.04	5.18	13.86
Gly 328	IIB-h2	13.71	0	13.71
Leu 331	IIB-h2	5.85	0.34	5.51
Ala 350	IIB-h3	17.2	11.05	6.15
Glu 354	IIB-h3	19.91	17.99	1.92

(b)

residues	domain	ASA_{HSA}	ASA_{HSA-PF^+}	ΔASA
Arg 209	IIA-h2	129.8	110.72	19.08
Ala 210	IIA-h2	25.81	25.6	0.21
Lys 212	IIA-h2	71.13	40.84	30.29
Ala 213	IIA-h2	35.05	14.53	20.52
Val 216	IIA-h2	15.02	0.2	14.82
Phe 228	IIA-h3	39.75	29.81	9.94
Ser 232	IIA-h3	37.04	14.08	22.96
Val 235	IIA-h3	4.93	0	4.93
Thr 236	IIA-h3	75.7	65.62	10.08
Asp 324	IIB-h2	76.96	46.71	30.25
Val 325	IIB-h2	84.55	74.41	10.14
Leu 327	IIB-h2	19.04	11.02	8.02
Gly 328	IIB-h2	13.71	0	13.71
Leu 331	IIB-h2	5.85	3.21	2.64

to observe appreciable MFE, i.e., the optimal distance and spin correlation between the radical ions formed as a result of PET. Previously our group reported that such a condition of pseudoconfinement is imposed by a partial intercalative mode of binding and the complex structure of DNA, which eventually leads to appreciable MFE in homogeneous medium.[60] Thus, owing to their complex structures, biomacromolecules have a unique potential to impart a confined and restricted environment to the RPs/RIPs that help them to maintain their spin correlation as well as the optimum distance of separation, so that appreciable MFE is observed even in homogeneous medium.

3.5. Docking Results. In order to substantiate the results obtained from spectroscopic studies, AY and PF$^+$ are docked to HSA. Docking studies indicate that both the ligands interact with residues belonging to subdomain IIA and also with some residues of subdomain IIB. Subdomain IIA contains the sole tryptophan residue (W214) of HSA, which is the major fluorophore of the protein. The detailed description of the interacting residues is given in Table 6a,b. It is evident from Table 6a,b that the total ASA of HSA lost on binding to AY is 40 Å^2 more than that with PF$^+$, implying that AY fits better into the binding pockets of HSA than PF$^+$. This is corroborated by the findings of the CD experiment, which show that AY perturbs the structure of the model protein more efficiently compared to PF$^+$.

Fluorescence spectrum of HSA shows a blue shift on addition of both AY and PF$^+$, indicating that Trp 214 experiences a more hydrophobic environment on binding with AY, which in turn is substantiated by the docking studies, which show that binding of the two acridine derivatives does not produce any change in the solvent ASA of Trp 214 (Table 6a,b). AY and PF$^+$ are found to be in close proximity to the hydrophobic residues Ala (210,213), Val (216,235), and Phe (228) of subdomain IIA, and Val (325), Leu (327,331), Gly (328), and Ala (350) of subdomain IIB. This suggests that van der Waals interactions are predominant in the binding, which supports the fluorescence results. Also, specific hydrogen bonding is possible. Furthermore, this finding provides a structural basis to explain the fluorescence quenching of HSA emission in the presence of the molecules. Possible hydrogen bonding distances between specific residues in the binding site of HSA and the two ligands are given in Table 7. In the case of AY-HSA system, the nitrogen atoms at 3 and 6 positions of AY are within hydrogen bonding distance from Arg 209 and Thr 236 of HSA. Similarly, in the case of the PF$^+$−HSA system, the nitrogen atom at the 3 position of PF$^+$ is within hydrogen bonding distance from Arg 209 of HSA and the nitrogen atom at the 6 position of PF$^+$ is within hydrogen bonding distance from Thr 236 as well as Ser 232 of HSA. Thus, in the case of the PF$^+$−HSA system, an additional amino acid residue (Ser 232) takes part in hydrogen bond formation, thus imparting extra stability to this system. One of the prime causes of the differential behavior of the two drugs toward HSA is the polar amino acid residue, Ser 232. It is to be noted from the findings of binding analysis (Table 4) that, at any particular temperature, the binding constant for the PF$^+$−HSA system is more than that for the AY−HSA system. Moreover, for both the PF$^+$−HSA and AY−HSA systems, the value of the binding constant decreases with increase in temperature probably because the complex formed loses its stability at higher temperature; however, the extent of decrease in binding constant is less for the PF$^+$−HSA system compared to the AY−HSA system. If we consider the docked poses of PF$^+$ with HSA, there appears to be a possibility for additional hydrogen bonding with Ser 232 (Table 7), which imparts an extra stability to the system. Hydrogen bonding with Ser 232 is absent in the case of the AY−HSA system. Additionally, the presence of the charge on PF$^+$ may also have an extra stabilizing effect for stronger binding compared to AY.

TABLE 7: Distances (in Å) between the Amino Acid Residues in the Binding Site of HSA and the Two Ligands

HSA	AY	PF$^+$
Arg 209 O	2.81 [3-N]	2.83 [3-N]
Thr 236 O	3.36 [6-N]	3.28 [6-N]
Ser 232 O		3.16 [6-N]

The predominance of hydrogen bonding as one of the key interacting forces as predicted from the signs of the thermodynamic parameters from fluorescence study of the PF$^+$−HSA system can be traced to the additional hydrogen bonding with Ser 232. Moreover, the preponderance of van der Waals interaction, predicted from the signs of thermodynamic parameters, in the PF$^+$−HSA system may also be due to the interaction of "charged" PF$^+$ moiety with the serine residue, which is a polar amino acid.

The stereoview of the docked conformations is presented in the Figure 9, which shows that the Trp−AY distance is 13.34 Å, while the Trp-PF$^+$ distance is 12.93 Å; whereas FRET calculations show that the experimental Trp−AY and Trp−PF$^+$ distances are 29.51 Å and 27.83 Å, respectively. The values of ligand−Trp distance obtained from experimental and docking studies shows slight discrepancies, although the trend (i.e., Trp−AY distance > Trp−PF$^+$ distance) is maintained well.

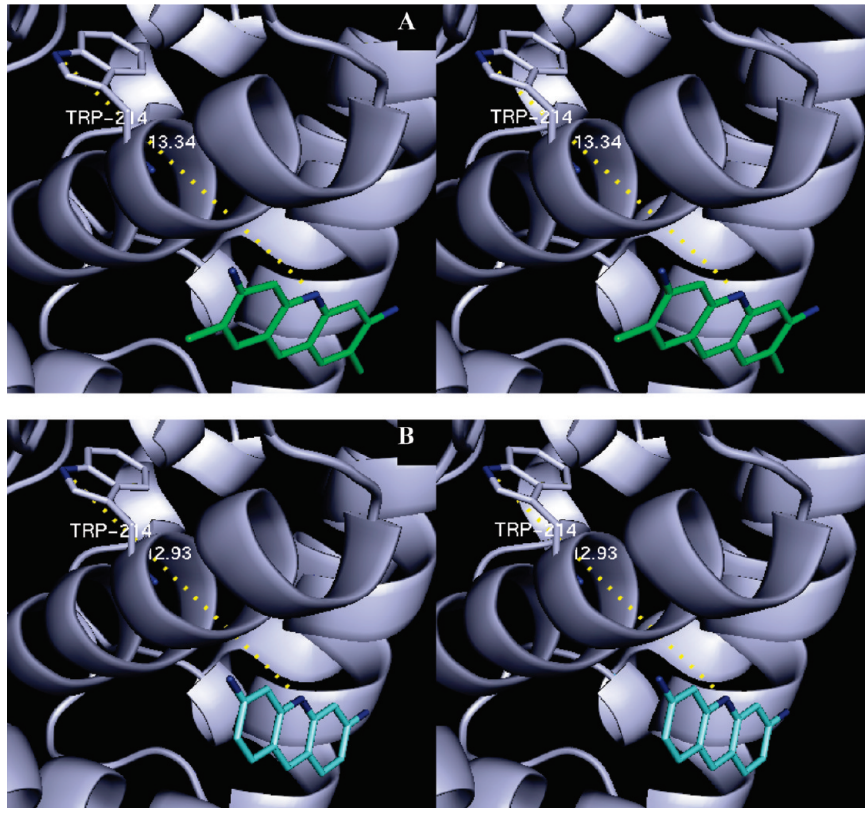

Figure 9. The stereoview of the docked conformations of HSA with (A) AY and (B) PF^+.

Now, fluorescence quenching for both these systems can be attributed to two phenomena, namely, energy transfer and PET; the latter has been confirmed from the laser flash photolysis method in conjunction with an external MF. Thus, energy transfer is not the sole cause of fluorescence quenching of HSA. However, protein−ligand distance obtained experimentally is based purely on the assumption of FRET, which is not the sole phenomenon responsible for fluorescence quenching. This may be the cause of the slight disagreement of the experimentally and theoretically obtained values of protein−ligand distance. Moreover, docking studies involve the attainment of optimized structure as well as the orientations of the drug and the protein molecules so that the total free energy of the system is minimized. Thus, minimum energy conformation is given more significance in this case, although the involvement of other conformations is also feasible. This may be another cause of discrepancy in the results of docking studies when compared to those of experimental ones, although the trends of distances obtained from docking and experimental studies agree well. As discussed in the introduction, MFE is observed mostly when the partner radicals/radical ions are separated by ∼10−20 Å. Since prominent MFE is obtained in both drug−protein systems, it may be assumed that the distances obtained from the docking studies is closer to the actual distances where PET occurs.

The ranking of the generated solutions in FlexX is performed using a scoring function that estimates the free binding energy (ΔG) of the protein−ligand complex considering various types of molecular interactions.[61] The equation uses the ΔG of an ideal hydrogen bond, ionic, aromatic, or lipophilic interaction, adjusted by a penalty function that depends on deviation from the ideal interatomic radius for the two interacting elements. From the docking studies we find that the total scores in the case of AY and PF^+ are −9.59 and −11.1, respectively, which are in good agreement with the ΔG^0 values (Table 4) of interaction with HSA. Hence, the fact that the interaction of PF^+ with HSA is more spontaneous than that of AY is supported by both the thermodynamics and the docking studies. The surface representations of the docked conformations are given in the following Figure 10.

Thus, it is found that while comparing the donor−acceptor distances and binding energies obtained from docking and experimental studies, the trend of the results obtained for both AY−HSA and PF^+−HSA are in agreement.

4. Conclusion

In this paper, we have made an attempt to explore the mechanism of interaction as well as the binding modes of two potent PDT photosensitizers, viz., AY and PF^+, with HSA, the most abundant carrier protein in human blood. The investigation is carried out spectroscopically as well as theoretically by docking methods. Simultaneous occurrence of FRET and PET are specifically highlighted in this study. The phenomenon of energy transfer is found to take place from the protein to the PDT drugs and has been utilized as a "spectroscopic ruler" to measure the distance between the ligands and the fluorophore in the protein. Use of the laser flash photolysis technique coupled with an external MF helps in identification of the transients, elucidation of the reaction mechanisms, and study of the spin dynamics, which eventually reveals that PET takes place from the tryptophan residue of HSA to the drugs, and the parent spin state of the precursors of electron transfer is triplet. It is noteworthy that the ground-state complex formed in both the systems undergoes ISC and reaches the triplet state, where it undergoes partial charge separation and finally shows MFE. The experimental findings have been substantiated by the results of docking studies. Docking study delineates the crucial role of Ser 232 residue of HSA in explaining the differential behavior

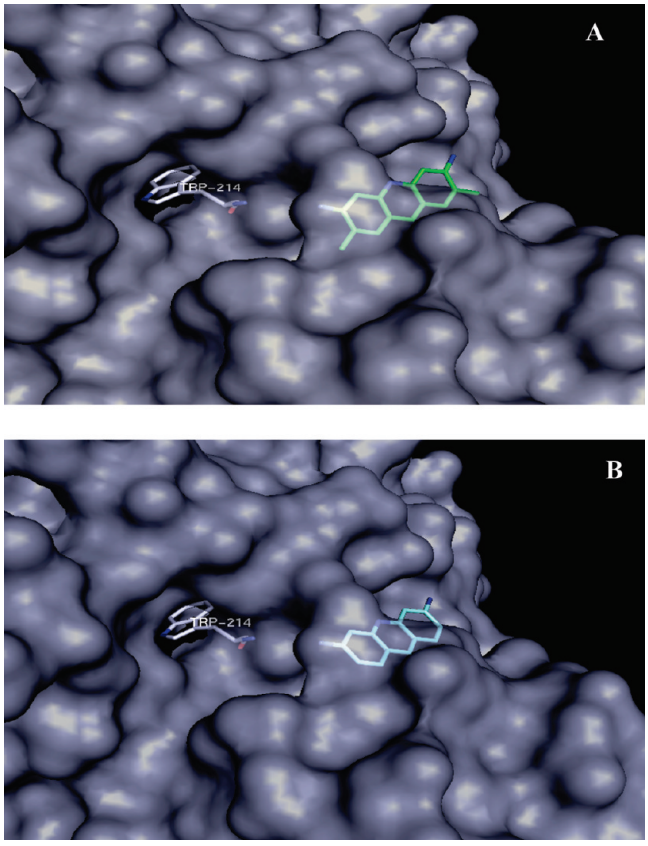

Figure 10. Surface representation of HSA showing the binding pockets of (A) AY and (B) PF^+.

of the two drugs towards the model protein. As already discussed in the Introduction, MFE is prominent when the partner radicals/radical ions in the geminate cage are within a separation distance of 10−20 Å. Docking study suggests that the Trp−AY distance is 13.34 Å, while the Trp−PF^+ distance is 12.93 Å. Thus, as the separation distances are suitable enough to preserve spin correlation, both the systems show substantial MFE. In one of our previous studies, which involved the interaction of hen-egg white lysozyme (HEWL) with menadione, it has been found that the distance between menadione and Trp 108 of HEWL is 2.79 Å.[51] In this case, Trp 108 is the residue that primarily interacts with menadione. However, it has been found that, on photoexcitation, PET takes place from HEWL to menadione, but no MFE is observed. This is possibly because of the extremely close vicinity (2.79 Å) of the electron donor (Trp 108) and the acceptor, where exchange interaction may hinder spin conversion. On the contrary, as the optimum distance between the radicals/radical ions is maintained in the present systems because of the restricted environment imposed by the structure of the protein, significant MFE is obtained in the presence of an external MF. This comparison highlights the importance of distance of separation between the solvent-separated radicals/radical ions in MFE, and, thus, an estimation of the proximity of the RPs/RIPs formed as a result of PET can be obtained from the study of MFE.

Acknowledgment. Financial assistance from the Molecular Mechanism of Diseases and Drug Action (MMDDA) project, SINP of Department of Atomic Energy (DAE), Government of India, is greatly acknowledged. We would like to acknowledge our thanks to Prof. Soumen Basak, SINP, for his guidance during CD experiments. We are also thankful to Mrs. Chitra Raha, SINP, Kolkata, for her assistance in flash photolysis experiments.

References and Notes

(1) Ahmad, B.; Parveen, S.; Khan, R. H. *Biomacromolecules* **2006**, *7*, 1350–1356.
(2) Patel, S.; Datta, A. *J. Phys. Chem. B* **2007**, *111*, 10557–10562.
(3) Sahoo, B. K.; Ghosh, K. S.; Dasgupta, S. *Biopolymers* **2009**, *91*, 108–119.
(4) Chakraborty, B.; Basu, S. *J. Lumin.* **2009**, *129*, 34–39.
(5) Morozova, O. B.; Hore, P. J.; Sagdeev, R. Z.; Yurkovskaya, A. V. *J. Phys. Chem. B* **2005**, *109*, 21971–21978.
(6) Kiger, L.; Marden, M. C. *J. Biol. Chem.* **2001**, *276*, 47937–47943.
(7) McLendon, G.; Hake, R. *Chem. Rev.* **1992**, *92*, 481–490.
(8) Winkler, J. R.; Gray, H. B. *Chem. Rev.* **1992**, *92*, 369–379.
(9) Lasey, R. C.; Liu, L.; Zang, L.; Ogawa, M. Y. *Biochemistry* **2003**, *42*, 3904–3910.
(10) Swanson, M. A.; Usselman, R. J.; Frerman, F. E.; Eaton, G. R.; Eaton, S. S. *Biochemistry* **2008**, *47*, 8894–8901.
(11) Buchachenko, A. L. *Chem. Rev.* **1995**, *95*, 2507–2528.
(12) Boxer, S. G.; Chidsey, C. E. D.; Roelofs, M. G. *Annu. Rev. Phys. Chem.* **1983**, *34*, 389–417.
(13) Gould, I. R.; Turro, N. J.; Zimmt, N. B. *Advances in Physical Organic Chemistry*; Academic Press: London, 1984; Vol. 20.
(14) Steiner, U. E.; Ulrich, T. *Chem. Rev.* **1989**, *89*, 51–147.
(15) Bhattacharya, K.; Chowdhury, M. *Chem. Rev.* **1993**, *93*, 507–535.
(16) Grissom, C. B. *Chem. Rev.* **1995**, *95*, 3–24.
(17) Scaiano, J. C.; Cozens, F. L.; Mohtat, N. *Photochem. Photobiol.* **1995**, *62*, 818–829.
(18) *Dynamic Spin Chemistry Magnetic Controls and Spin Dynamics of Chemical Reactions*; Nagakura, S., Hayashi, H., Azumi, T., Eds.; Kodansha, Ltd.: Tokyo, 1998.
(19) Tanimoto, Y., Fujiwara, Y. *Handbook of Photochemistry and Photobiology: Inorganic Chemistry*; Nalwa, H. S., Ed.; American Scientific Publishers: Stevenson Ranch, CA, 2003; Vol 1.
(20) Turro, N. J.; Weed, G. C. *J. Am. Chem. Soc.* **1983**, *105*, 1861–1868.
(21) Dutta Choudhury, S.; Basu, S. *J. Phys. Chem. A* **2005**, *109*, 8113–8120.
(22) Scaiano, J. C.; Cozens, F. L.; McLean, J. *Photochem. Photobiol.* **1994**, *59*, 585–589.
(23) Fritsch, C.; Goerz, G.; Ruzicka, T. *Arch. Dermatol.* **1998**, *134*, 207–214.
(24) Varnell, E. D.; Kaufman, H. E. *Infect. Immun.* **1973**, *7*, 518–519.
(25) Satonaka, H.; Kusuzaki, K.; Matsubara, T.; Shintani, K.; Wakabayashi, T.; Nakamura, T.; Matsumine, A.; Uchida, A. *Anticancer Res.* **2007**, *27*, 3339–3344.
(26) Gilleland, G.; Bender, M. L. *J. Biol. Chem.* **1976**, *251*, 498–502.
(27) Glazer, A. N. *Proc. Natl. Acad. Sci. U.S.A.* **1965**, *54*, 171–176.
(28) Feng, S.; Shi, S. *Spectrochim. Acta, Part A* **2007**, *68*, 244–249.
(29) Lee, W. E.; Galley, W. G. *Biophys. J.* **1988**, *54*, 627–635.
(30) Lober, G.; Schutz, H.; Kleinwatcher, V. *Biopolymers* **1972**, *11*, 2439–2459.
(31) Long, Y. F.; Huang, C. Z.; Li, Y. F. *J. Phys. Chem. B.* **2007**, *111*, 4535–4538.
(32) *Albumin Structure, Function and Uses*; Rosenoer, V. M., Oratz, M., Rothschild, M. A., Eds.; Pergamon: Oxford, U.K., 1977.
(33) Bertucci, C.; Domernici, E. *Curr. Med. Chem.* **2002**, *9*, 1463–1481.
(34) Li, J.; Ren, C.; Zhang, Y.; Liu, X.; Yao, X.; Hu, Z. *J. Mol. Struct.* **2008**, *885*, 64–69.
(35) Moreno, F.; Cortijo, M.; Jimenez, J. G. *Photochem. Photobiol.* **1999**, *70*, 695–700.
(36) Lakowicz, J. R. *Principles of Fluorescence Spectroscopy*, 2nd ed.; Kluwer Academic/Plenum Publishers: New York, 1999.
(37) Gao, H.; Lei, L.; Liu, J.; Kong, Q.; Chen, X.; Hu, Z. *Photochem. Photobiol. A* **2004**, *167*, 213–221.
(38) Maiti, T. K.; Ghosh, K. S.; Samanta, A.; Dasgupta, S. *Photochem. Photobiol. A* **2008**, *194*, 297–307.
(39) Berman, H. M.; Westbrook, J.; Feng, Z.; Gilliland, G.; Bhat, T. N.; Weissig, H.; Shindyalov, I. N.; Bourne, P. E. *Nucleic Acids Res.* **2000**, *28*, 235–242.
(40) DeLano, W. L. *The PyMOL Molecular Graphics System*; DeLano Scientific: San Carlos, CA, 2004, http://pymol.sourceforge.net/.
(41) Hubbard, S. J.; Thornton, J. M. *'NACCESS' Computer Program*; Department of Biochemistry and Molecular Biology, University College: London, 1993.
(42) Pimentel, G. C. *J. Am. Chem. Soc.* **1957**, *79*, 3323–3326.
(43) Mamedov, F. D.; Salimov, M. A. *J. Appl. Spectrosc.* **1971**, *14*, 333–335.
(44) Strickland, E. H.; Wilchek, M.; Horwitz, J.; Billups, C. *J. Biol. Chem.* **1972**, *247*, 572–580.
(45) Ware, W. R. *J. Phys. Chem.* **1962**, *66*, 455–458.
(46) Wang, C. X.; Yan, F. F.; Zhang, Y. X.; Ye, L. *J. Photochem. Photobiol. A* **2007**, *192*, 23–28.

(47) Zhou, N.; Liang, Y. Z.; Wang, P. *J. Photochem. Photobiol. A* **2007**, *185*, 271–276.
(48) Barik, A.; Mishra, B.; Kunwar, A.; Priyadarsini, K. I. *Chem. Phys. Lett.* **2007**, *436*, 239–243.
(49) Maiti, T. K.; Ghosh, K. S.; Samanta, A.; Dasgupta, S. *J. Photochem. Photobiol. A* **2008**, *194*, 297–307.
(50) Ross, P. D.; Subhramanian, S. *Biochemistry* **1981**, *20*, 3096–3102.
(51) Banerjee, S.; Dutta Choudhury, S.; Dasgupta, S.; Basu, S. *J. Lumin.* **2008**, *128*, 437–444.
(52) Bent, D. V.; Hayon, E. *J. Am. Chem. Soc.* **1975**, *97*, 2612–2619.
(53) Creed, D. *Photochem. Photobiol.* **1984**, *39*, 537–562.
(54) Chakraborty, B.; Basu, S. *Chem. Phys. Lett.* **2009**, *477*, 382–387.
(55) Chakraborty, B.; Basu, S. *Chem. Phys. Lett.* **2010**, *487*, 51–57.
(56) Dutta Choudhury, S.; Basu, S. *J. Phys. Chem. B* **2006**, *110*, 8850–8855.
(57) Plleni, M. P.; Gratzel, M. *J. Phys. Chem.* **1980**, *84*, 2402–2406.
(58) Chakraborty, B.; Basu, S. *Chem. Phys. Lett.* **2010**, *493*, 76–82.
(59) Wakasa, M.; Hayashi, H.; Mikami, Y.; Takeda, T. *J. Phys. Chem.* **1995**, *99*, 13181–13186.
(60) Dey, D.; Pramanik, N. R.; Basu, S. *J. Phys. Chem. B* **2009**, *113*, 8689–8694.
(61) Rarey, M.; Kramer, B.; Lengauer, T.; Klebe, G. *J. Mol. Biol.* **1996**, *261*, 470–489.

JP109604A